Group 14 Methylene–Methane-type Complexes: A Theoretical Study

Georges Trinquier
Laboratoire de Physique Quantique, C.N.R.S. U.R.A. 505, I.R.S.A.M.C., Université Paul-Sabatier, 31062 Toulouse Cedex, France

Neutral complexes between Group 14 singlet methylene- and methane-type fragments, $H_3X{-}H\cdots XH_2$, have been investigated by *ab initio* calculations. Beyond carbon, such singly bridged complexes are found to be significantly bound, as has recently been reported for silicon. At our best level of treatment (MP4 energies on SCF-DZP geometries), the binding energies relative to the set $XH_4 + XH_2$ range from 5 to 10 kcal mol^{-1} from silicon to lead. Starting from these complexes, the pathways for methylene insertion into methane are examined for carbon and all its analogues. The rearrangement $H_3X{-}H{-}XH_2 \rightarrow H_3X{-}XH_3$ becomes less exothermic with heavier elements. The corresponding energy differences range from 49 to 9 kcal mol^{-1} from silicon to lead. This is on a par with increasing energy barriers, which are calculated to be near zero for carbon and silicon, and increases up to 20 kcal mol^{-1} for lead. Other aspects of the X_2H_6 potential surfaces are discussed, in particular a low-energy saddle point is found for hydrogen exchange between SiH_4 and SiH_2.

In a recent discussion on non-symmetrical hydrogen bridges in main-group chemistry, it was noted that to favour the formation of a three-centre two-electron bridge X—H—Y from X—H + Y fragments, compensation must somehow take place to balance the partial migration of the X—H electron pair towards the acceptor orbital at Y.[1] In ionic systems such as the isomers **1** and **2** of the

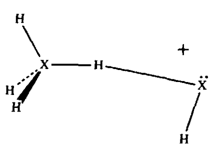

1

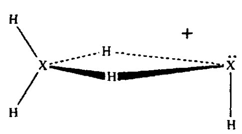

2

ethyl cation analogues, this is achieved by the formal positive charge at the XH^+ fragment. In these cases, the binding energies with respect to $XH_4 + XH^+$ may reach significant values (30–40 kcal mol^{-1}† for X = Si to Pb).[2] If we now consider the only possibility (within a non-hypervalent scheme) for building a hydrogen bridge between a methane-like neutral fragment XH_4 and a singlet methylene-like fragment $:XH_2$ (bearing an empty p_π orbital), **3**, only a weakly bound complex is

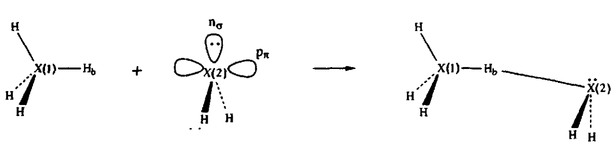

3

expected. Still, the corresponding binding energy may be enhanced provided that the H_b and X(2) atoms in the starting fragments carry prominent net charges, negative and positive, respectively. This cannot occur with carbon because of the $C^-{-}^+H$ bond polarity. It is however, expected with the heavier analogues in Group 14, which all exhibit marked $X^+{-}^-H$ bond polarities. This has been exemplified by Pb_2H_6, for which the bridged form was calculated to be bound by *ca.* 9 kcal mol^{-1}. Recently, a similar bridged complex has also been reported as a bound intermediate in the potential entrance channel for the insertion reaction of silylene into silane.[3] Such a complex is much higher in energy than the stable disilane form, so the corresponding barrier between them is very small. We thought that with heavier atoms of Group 14, the energy difference between the ethane-like form $H_3X{-}XH_3$ and the complex $H_3X{-}H{-}XH_2$ could be reduced, inducing a higher barrier between them, in the spirit of the Hammond postulate.

In this work, we have undertaken a theoretical study of the X_2H_6 potential-energy surfaces for the whole of Group 14, focusing on the energy profile for the dissociation (or insertion) recaction:

$$H_3X{-}XH_3 \rightarrow XH_4 + :XH_2\ (^1A_1)$$

Some additional aspects will be addressed, which complete the view of this part of the X_2H_6 potential surfaces, namely the rotational barrier in the ethane-like form, its dissociation into $2XH_3$, and hydrogen exchange between XH_4 and XH_2.

Our *ab initio* calculations use effective core potentials to describe the core electrons. For tin and lead atoms, these potentials take into account the mean relativistic effects. All geometries are optimized at the Hartree–Fock level, using valence basis sets of double-zeta + polarization quality. MP4 calculations are performed on these geometries in order to obtain energetics where a large part of the correlation effects are taken into account. Further technical details are given in the Appendix. The paper will first deal with the structure of the bridged complex for X_2H_6, and its comparison with that for $X_2H_5^+$. Then the energy profiles for the whole insertion reaction are discussed. Lastly, we will briefly adress the mechanism for hydrogen exchange between XH_4 and XH_2.

Structures

The geometrical parameters for the two forms of X_2H_6 are listed in Table 1, together with those of the fragments XH_3, XH_2 and XH_4 involved in this work. The harmonic vibrational frequencies for the ethane-like and the bridged structures of X_2H_6 are listed in Table 2.

Owing to the intermolecular nature of the $H_3XH_b{-}XH_2$ link, the potential-energy surface is very flat, in particular with respect to the rotations around the bonds that make up the X(1)—H_b—X(2) link. Basically, there are two conformations that can be obtained when the complex is constrained

† 1 cal ≈ 4.184 J.

Table 1 Calculated geometries[a]

		C	Si	Ge	Sn	Pb
XH_2 (C_{2v})	HXH	102.5	93.7	93.0	92.5	92.0
	X—H	1.106	1.508	1.597	1.768	1.832
XH_4 (T_d)	X—H	1.092	1.473	1.547	1.710	1.740
$^{\bullet}XH_3$ (C_{3v})	X—H	1.082	1.474	1.549	1.717	1.760
	HXH	120.0	111.1	110.7	109.4	109.1
$H_3X—XH_3$ (D_{3d})	X—X	1.526	2.347	2.497	2.797	2.836
	X—H	1.094	1.477	1.549	1.714	1.746
	HXH	107.6	108.8	108.7	108.4	108.5
$H_3X—XH_3$ (D_{3h})	X—X	1.541	2.357	2.505	2.803	2.842
	X—H	1.093	1.476	1.549	1.713	1.746
	HXH	107.1	108.6	108.6	108.3	108.4
$H_3X—H—XH_2$ [b]	X(1)—H_b	1.092	1.490	1.569	1.756	1.784
	X(2)—H_b	2.838	2.132	2.222	2.119	2.337
	X(1)—H(1)	1.093	1.467	1.538	1.697	1.724
	X(1)—H(2)	1.091	1.469	1.542	1.709	1.731
					1.702	1.740
	X(2)—H(3)	1.105	1.509	1.598	1.768	1.841
					1.776	1.834
	X(1)—X(2)	3.572	3.547	3.615	3.529	3.731
	X(1)H_bX(2)	124.4	156.4	144.4	131.0	129.3
	H(1)X(1)H_b	110.2	109.2	110.0	111.7	110.3
	H(2)X(1)H_b	109.3	107.2	106.6	102.5	103.6
					106.9	107.2
	H(2)X(1)H(2)	109.6	110.9	110.9	110.8	110.8
	H_bX(2)H(3)	94.4	84.6	85.4	85.4	83.0
					83.4	85.3
	H(3)X(2)H(3)	102.6	94.1	93.3	92.4	91.6

[a] In Å and degrees. The actual symmetry of $^{\bullet}CH_3$ is D_{3h}. [b] The minimum has C_s symmetry for carbon, silicon and germanium, and C_1 symmetry for tin and lead.

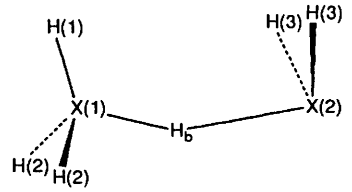

Table 2 Harmonic vibrational frequencies (in cm^{-1})

	C	Si	Ge		Sn	Pb
			$H_3X—XH_3$			
$1a_{1u}$	340	145	110		81	73
$1e_u$	888	434	386		329	310
$1a_{1g}$	1048	463	264		191	137
$1e_g$	1323	704	610		504	477
$1a_{2u}$	1498	955	846		731	660
$2e_g$	1598	1033	953		816	785
$2a_{1g}$	1545	1039	934		820	786
$2e_u$	1606	1051	962		823	791
$2a_{2u}$	3148	2318	2184		2059	1918
$3e_g$	3205	2321	2165		2043	1909
$3e_u$	3232	2330	2173		2050	1919
$3a_{1g}$	3157	2333	2199		2073	1935
			$H_3X—H—XH_2$			
1a″	56	48	47	1a′	60	45
1a′	43	54	60	2a′	138	124
2a″	127	139	115	3a′	164	145
2a′	116	181	217	4a′	336	282
3a″	173	511	465	5a′	490	406
3a′	247	567	505	6a′	525	456
4a′	1440	1007	888	7a′	760	713
4a″	1438	1033	910	8a′	802	756
5a′	1449	1040	939	9a′	813	771
5a″	1649	1052	972	10a′	823	791
6a′	1502	1055	992	11a′	875	823
7a′	1655	1111	1008	12a′	1031	913
6a″	3165	2152	1972	13a′	1829	1649
8a′	3111	2167	1989	14a′	1858	1677
9a′	3150	2224	2042	15a′	1873	1758
10a′	3258	2374	2226	16a′	2094	1957
7a″	3273	2377	2215	17a′	2109	1988
11a′	3266	2385	2246	18a′	2127	2007

to C_s symmetry. These are **4** and **5**, and may be labelled *syn* and *anti* due to the relative arrangement of

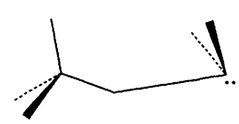

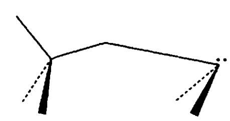

4 **5**

the necessarily coplanar atoms H(1)—X(1)—H_b—X(2). Note that the methylene group XH_2 always takes a *cis* orientation with respect to the X(1)—H_b bond, in order to optimize the interactions between the two corresponding dipoles. A similar trend was also observed in $H_3X—H—XH^+$. The energy differences between **4** and **5** are very small, but the *syn* form **4** is always preferred over the *anti* form **5**, which in all cases exhibits one imaginary frequency. Structure **4** in C_s symmetry corresponds to the complex's true minimum for C_2H_6, Si_2H_6 and Ge_2H_6. In the remaining heavier analogues, the structure looses its C_s symmetry by slightly distorting towards a C_1 arrangement. Anyway, these forms are quite close in energy (the difference between **4** and **5** is always less than 0.1 kcal mol^{-1}). The conformations that are best prepared for the methylene insertion and that prefigure the corresponding transition states are **6** and **7**, which are also within some tenths of a kcal mol^{-1} above the preferred forms.

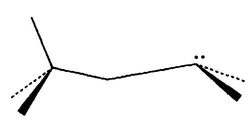

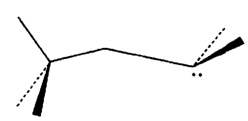

6 **7**

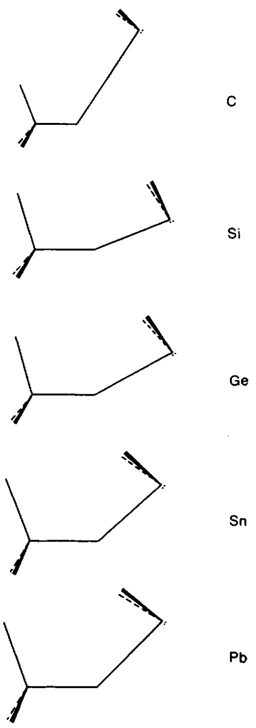

Fig. 1 Bridged structures of X_2H_6 in their favoured *syn* conformation

The optimized geometries for conformation **4** are depicted in Fig. 1 and those corresponding to conformation **5** are given in Fig. 2 and compared to the similar *anti* arrangement preferrentially obtained for $H_3X{-}H{-}XH^+$. For carbon, both from energetic and geometrical grounds, the bridged complex should not exist. First, it is no longer bound when the zero-point vibrational energies are taken into account and secondly one can see in Table 1 and Fig. 1 and 2 that the

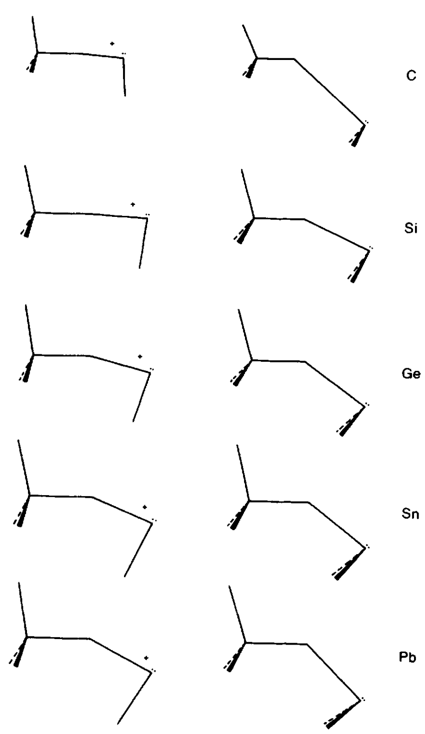

Fig. 2 Bridged structures of $X_2H_5^+$ and X_2H_6 in their *anti* conformation

$H_b{-}C(2)$ bond is quite long [only 0.1 Å shorter than the sum of the van der Waals radii (2.9 Å)] while the $C(1){-}H_b$ distance remains unchanged with respect to that in CH_4.

For silicon, our SCF-optimized geometry corresponds to a bridged structure that is less bound than that obtained by Becerra *et al.* at the MP2 level of optimization.[3] This is seen from the pair of $X{-}H_b$ distances calculated to be 1.57/1.69 Å and 1.52/2.05 Å at the MP2 level, depending on the basis set, while the present values are only 1.49/2.13 Å. The MP2 geometry was found to be of C_1 symmetry, while our SCF geometry has C_s symmetry and we have carefully checked that any C_1-distorted structure does relax towards a C_s structure. The extreme flatness of the surface is further illustrated by the divergence of the valence angles at the bridging hydrogen. Depending on the basis set used, the MP2 value varies from 121° (DZP) to 86° (TZP),[3] while our SCF value is 156°. Because the bridged structure is basically an intermolecular complex, the MP2 correlated treatment led to a more compact and bound structure since it accounts better for the van der Waals interactions, whereas the SCF level accounts only for the charge-transfer and delocalization components. Anyway, in the present work the structural discussion is mainly comparative along the series and the SCF description of the geometries should be sufficient for that.

In the bridged complex, the XH_4 and XH_2 fragments basically preserve their geometries. The small changes become more and more marked along the series as can be seen from the lengthening of the $X(1){-}H_b$ bond with respect to that in XH_4. Lengthening remains small and regularly increases from 1.2% (Si) to 2.6% (Pb). Discarding the case of carbon, the tilting of the $:XH_2$ group becomes more and more pronounced along the series, reflecting an increasing propensity to make the $X(1){-}H_b$ and XH_2 dipoles parallel [see Fig. 1 and 2 (right-hand side)].

The structural comparison between $H_3X{-}H{-}XH^+$ and $H_3X{-}H{-}XH_2$ indicates that the fragments are more tightly bound in the former ionic complex. The above-mentioned relative lengthening of $X(1){-}H_b$ is 7–9% in the ionic complex instead of 1–3% in the neutral complex. Similarly, the $X(1){-}H_b/H_b{-}X(2)$ ratio is around 90% in $X_2H_5^+$ while it is only 70–80% in X_2H_6. These effects are clearly paralleled by the calculated $X{-}H_b$ stretching force constants. Typical cases are given in the following table (in mdyn $Å^{-1}$).

		XH_4	X_2H_6	$X_2H_5^+$
C	$X(1){-}H_b$	5.79	5.80	
	$H_b{-}X(2)$		0.01	
Si	$X(1){-}H_b$	3.17	2.97	1.68
	$H_b{-}X(2)$		0.08	0.84
Pb	$X(1){-}H_b$	2.24	2.00	1.20
	$H_b{-}X(2)$		0.22	0.61

This shows the decrease in the $X(1){-}H_b$ bond strength and the increase in the $H_b{-}X(2)$ bond strength from Si_2H_6 to Pb_2H_6. In any case, $X(1){-}H_b$ remains close to the $X{-}H$ bond in XH_4, while the $H_b{-}X(2)$ bond remains weak. This is no longer true for $X_2H_5^+$. Note also the peculiarity of C_2H_6, for which the $C(1){-}H_b$ force constant is equal to that in CH_4, while the $H_b{-}C(2)$ force constant is typically that of a neutral van der Waals well. Fig. 1 shows that the tilting of the XH group in the cation is weaker than that of the XH_2 group in the neutral complex, although the trend to stronger tilting along the series is preserved in both cases. Lastly, the strength of the bonding between the fragments is further illustrated by the global charge transfer from XH_4. This results from delocalization effects described at the SCF level, and may be seen in the Mulliken analyses given in Table 3. The resultant charge that has migrated from XH_4 is indicated at

Table 3 Mulliken net atomic charges (e)

		C	Si	Ge	Sn	Pb
$^{\cdot}XH_3$	X	−0.18	+0.51	+0.36	+0.55	+0.42
	H	+0.06	−0.17	−0.12	−0.18	−0.14
XH_2	X	−0.07	+0.41	+0.31	+0.45	+0.42
	H	+0.03	−0.20	−0.16	−0.23	−0.21
XH_4	X	−0.10	+0.76	+0.54	+0.78	+0.58
	H	+0.03	−0.19	−0.14	−0.19	−0.15
$H_3X{-}XH_3$	X	−0.06	+0.51	+0.37	+0.57	+0.44
	H	+0.02	−0.17	−0.12	−0.19	−0.14
$H_3X{-}H{-}XH_2$	X(1)	−0.12	+0.86	+0.61	−0.86	+0.67
	X(2)	−0.07	+0.38	+0.29	+0.41	+0.39
	H_b	+0.04	−0.36	−0.24	−0.29	−0.25
	H(1)	+0.02	−0.16	−0.10	−0.14	−0.12
	H(2)	+0.03	−0.16	−0.11	−0.18	−0.24
					−0.16	−0.14
	H(3)	+0.03	−0.20	−0.17	−0.26	−0.24
					−0.24	−0.22
Total transfer from XH_4		−0.00	0.02	0.05	0.08	0.07

the bottom of Table 3. In the cationic complexes $H_3X{-}H{-}XH^+$, such electron transfers were about four times stronger.

We shall not comment on the geometries of the ethane-like forms or on those of the various fragments reported in Table 1, since they are no longer new. The agreement with the available experimental data is reasonable. The case of distannane has been previously discussed by Fernandez-Sanz and Marquez in a treatment that uses the same pseudopotentials and basis sets as ours.[4] Incidentally, these authors have shown that correlation effects do not affect the SCF-calculated geometry significantly. The case of diplumbane has not been discussed much, to our knowledge. A few X-ray structures of diplumbane derivatives bearing cyclohexyl or aromatic substituents are available, and exhibit PbPb distances of 2.84–2.88 Å.[5–7] Our value of 2.84 Å calculated for Pb_2H_6 is in reasonable agreement. A regular feature that appears in Table 1 for the ethane forms is the expected XX lengthening from the staggered D_{3d} conformation to the eclipsed D_{3h} conformation, while XH and HXH remain nearly unchanged.

Energies

The calculated relative energies are listed in Table 4, not taking into account the zero-point vibrational energy differences (ZPE). Comparison between the SCF and MP4 results shows that the energy differences between $H_3X{-}H{-}XH_2$ and $H_3X{-}XH_3$ are not affected much by the correlation effects which expectedly enhance the binding energies both for the bridged forms with respect to $XH_4 + XH_2$, and for the ethane form with respect to $2XH_3$.

Table 4 Relative energies (kcal mol^{-1})

	C	Si	Ge	Sn	Pb
		SCF			
$2^{\cdot}XH_3$	68.8	56.5	49.6	46.8	39.0
$XH_4 + XH_2$	96.9	49.3	37.9	31.0	13.5
$H_3X{-}H{-}XH_2$	96.6	47.6	36.3	25.6	8.6
$H_3X{-}XH_3$	0.0	0.0	0.0	0.0	0.0
		MP4			
$2^{\cdot}XH_3$ [a]	93.5	69.6	64.2	58.5	50.8
$XH_4 + XH_2$	110.9	53.3	41.4	33.6	17.9
$H_3X{-}H{-}XH_2$	109.8	48.5	36.3	23.8	8.8
$H_3X{-}XH_3$	0.0	0.0	0.0	0.0	0.0

[a] The $2XH_3$ radical set is located with respect to $H_3X{-}XH_3$ at the MP2 level only.

As expected, the difference between the bridged form $H_3X{-}H{-}XH_2$ and the ethane-like form $H_3X{-}XH_3$ regularly decreases from silicon to lead. For lead it is only 9 kcal mol^{-1}, while for carbon it is very large, more than twice than that of silicon. This partly (only partly, see below) reflects the strengths of the XX bond energies in $H_3X{-}XH_3$. A measure of these XX bond energies is given by the calculated energies for the homolytic dissociation of $H_3X{-}XH_3$ into $2XH_3$. For carbon and silicon, our MP2 estimates are in rough agreement with more accurately calculated ones.[8–13] Although these values are larger than the usual mean bond energies,[14] they reproduce the gap between C and Si, and the regular decrease from Si to Pb, as shown in the following (in kcal mol^{-1}).

	MP2	mean
C	94	83
Si	70	54
Ge	64	45
Sn	59	36
Pb	51	

The rotational barriers in $H_3X{-}XH_3$ are listed in Table 5. The present values are in agreement with those calculated previously.[4,15,16] Correlation effects increase the rotational barrier for ethane and disilane, while they decrease it by 0.1 kcal mol^{-1} for digermane to diplumbane. The zero-point vibrational energy differences further reduce the barriers by 0.1 kcal mol^{-1}, leading to a value of 0.2 kcal mol^{-1} for diplumbane.

The saddle points relating the bridged form to the ethane-like form have been determined for C_2H_6, Si_2H_6 and Pb_2H_6. They correspond to the transition state in the insertion reaction of methylene into methane. This problem is well documented not only for carbon, but also for silicon, for which the insertion of silylene into the SiH bond of silane or disilane has been theoretically explored.[17–20] For C_2H_6 and Si_2H_6, the determination of the transition state at the SCF level gives a significant barrier. Applying a correlated treatment such as MP3 or MP4 on these SCF transition structures makes the barrier vanish.[17] A more refined determination of the saddle point for Si_2H_6 has given a barrier of 1.5 kcal mol^{-1} [MP2/6-311G(d,p)].[3]

The energy barriers associated with the SCF-determined transition states for C, Si and Pb are listed in Table 6. In agreement with the above-mentioned data, we found for carbon and silicon significant barriers at the SCF level (16 and 9 kcal mol^{-1}) that both vanish at the MP4 level. For lead, the barrier is calculated at 29 kcal mol^{-1} at the SCF level and at 20 kcal mol^{-1} at the MP4 level. As previously noted in the isomerization path of $X_2H_5^+$, the height of the barrier with respect to the mid-distance between the two ends of the path is roughly the same for Si and Pb (32.5 and 32.8 kcal mol^{-1} at the SCF level, 24.1 and 24.5 kcal mol^{-1} at the MP4 level). This enables us to interpolate the barriers for Ge and Sn. Finally, barriers of 0, 6, 12 and 20 kcal mol^{-1} are obtained for Si, Ge, Sn and Pb. Taking into account the zero-point vibrational energies would further reduce these values by 0.4–0.8 kcal mol^{-1}. Our results therefore suggest that beyond silicon a significant barrier is required for the intramolecular rearrangement $H_3X{-}H{-}XH_2 \rightarrow H_3X{-}XH_3$. For

Table 5 Calculated rotational barriers in $H_3X{-}XH_3$ (kcal mol^{-1})

	C	Si	Ge	Sn	Pb
SCF	3.2	1.0	0.7	0.5	0.4
MP4	3.3	1.1	0.6	0.4	0.3
MP4 + ZPE	2.9	1.0	0.5	0.3	0.2

Table 6 Calculated energy barriers for the rearrangement $H_3X{-}H{-}XH_2 \rightarrow H_3X{-}XH_3$ [a]

		C	Si	Ge	Sn	Pb
	$H_3X{-}H{-}XH_2$	0.0	0.0	0.0	0.0	0.0
SCF	TS	16.4	8.7	14.5	19.7	28.5
	$H_3X{-}XH_3$	−96.6	−47.6	−36.3	−25.6	−8.6
MP4	TS	−0.5	−0.2	6.1	12.4	20.1
	$H_3X{-}XH_3$	−109.8	−48.5	−36.3	−23.8	−8.8

[a] In kcal mol^{-1}. TS stands for transition state. For Ge and Sn, the barriers are estimated through interpolation from Si to Pb (see text). MP4 energies correspond to SCF-determined structures.

lead, this barrier is as high as 20 kcal mol^{-1}, which is more than twice the exothermicity of the rearrangement. The corresponding pathways for all Group 14 systems are schematized in Fig. 3.

If we now consider the whole pathway from the fragments $XH_4 + XH_2$ to the ethane-like form $H_3X{-}XH_3$, the barrier for the insertion reaction must take into account the previous exothermicity for the formation of the bound complex. In this way, we still obtain no barrier for C or Si, and barriers of 1.0, 2.6 and 11.0 kcal mol^{-1} for Ge, Sn and Pb. Taking into account the zero-point energy differences would enhance these barriers to 3, 4 and 12 kcal mol^{-1}.

A global schematic representation of the surfaces is given in Fig. 4. According to a now familiar convention,[2,21] on the right-hand asymptote we locate the fragments arising from the 'natural' dissociation of the bridged form ($XH_4 + XH_2$) at a common zero energy, and on the left-hand asymptotes those corresponding to the 'natural' dissociation of the ethane-like form ($2XH_3$). In Fig. 4 we have used our MP4-calculated energies, except for the right-hand dissociation

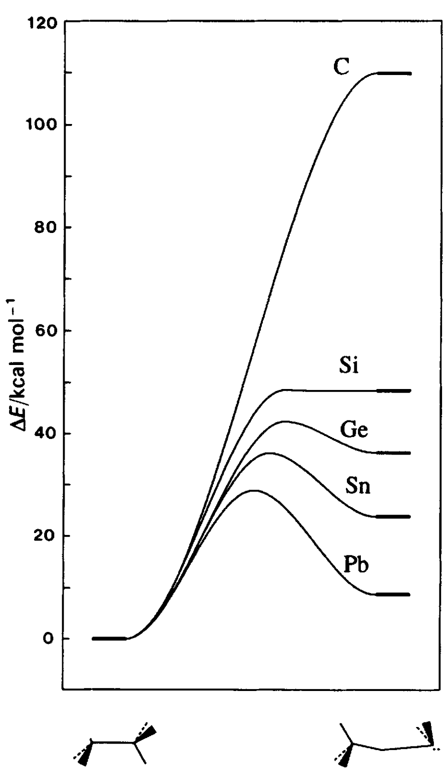

Fig. 3 Energy profiles for the interconverion of $H_3X{-}XH_3$ into $H_3X{-}H{-}XH_2$

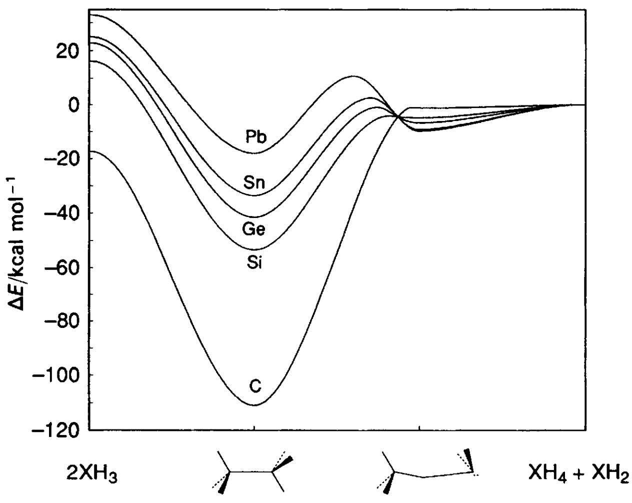

Fig. 4 Schematic representation of the X_2H_6 potential surfaces, using various cross-sections along a single coordinate. The right-hand asymptote, corresponding to the fragments $XH_4 + XH_2(^1A_1)$, is taken as a common zero energy. MP4 energies are used except for the homolytic dissociation into $2XH_3$ (left-hand asymptote) which is calculated at the MP2 level

curves, which correspond to MP2 energy differences between $2XH_3$ and $H_3X{-}XH_3$. For silicon, we have added a small barrier for clarity. This picture shows the regular trend in the shapes of the surfaces from Si to Pb. Here, carbon is not dramatically different from the other atoms, unlike the cases of X_2H_4, X_2F_4 and $X_2H_5^+$, except that the stable form, which contains a CC bond, is much more stable than any other form or fragment.

It is interesting to have a close look at the relative positions of the two sets of fragments at the two ends of Fig. 4. The energy for the disproportionation reaction $XH_2(^1A_1) + XH_4 \rightarrow 2XH_3$ is calculated as follows at two levels of theory (in kcal mol^{-1}).

	UHF	MP2
C	−30.1	−22.4
Si	7.2	14.0
Ge	11.7	20.3
Sn	15.8	23.1
Pb	25.5	31.3

The methyl-like fragments are favoured only for carbon. From silicon to lead, the methylene + methane-like set becomes more and more favoured. The final rationalization of the $H_3X{-}XH_3/H_3X{-}H{-}XH_2$ energy differences should be understood not only on XX bond energy grounds, but also from these disproportionation energies. We have tried to summarize this, at the MP2 level, in Fig. 5: (*a*) corresponds to the energy of the dismutation reaction $XH_4 + XH_2 \rightarrow 2XH_3$; (*b*) corresponds to the energy of the association reaction $2XH_3 \rightarrow H_3X{-}XH_3$; (*c*) is (*b*) minus the energy for the association reaction $XH_4 + XH_2 \rightarrow H_3X{-}H{-}XH_2$, *i.e.* the differential binding energy of the ethane-like and bridged forms relative to their respective 'natural' dissociation products; finally, the bold curve is the sum of (*a*) and (*c*), and corresponds to the energy for the rearrangement $H_3X{-}H{-}XH_2 \rightarrow H_3X{-}XH_3$. Although the XX bond energy (*c*) slightly predominates, both effects are equally important for the resulting curve. Note also that (*b*) and (*c*) are very close, which reflects the fact that bond energies in the X−H−X bridges are much smaller than those in the X−X bonds.

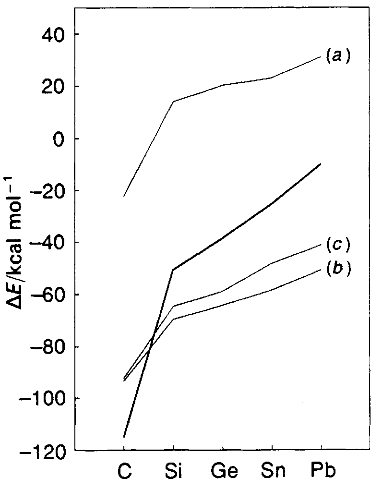

Fig. 5 Decomposition of the MP2 energy for the rearrangement of the bridged form into the ethane-like form: (*a*) energy for the disproportionation of $XH_4 + XH_2$ into $2XH_3$; (*b*) energy for the reaction $2XH_3 \rightarrow H_3X{-}XH_3$; (*c*) same as (*b*) minus the energy for the reaction $XH_4 + XH_2 \rightarrow H_3X{-}H{-}XH_2$. The final result (bold line) corresponds to (*a*) + (*c*)

Can we rationalize the $H_3X{-}XH_3/H_3X{-}H{-}XH_2$ energy differences through the simplified additive systematics proposed in ref. 2? Obviously not, since this model assumes that the bond energy for the X—H—X bridge is the sum of the X—H energy and a constant increment, called BBB, which is the binding energy when making X—H—X from X—H + X. In our case, this would correspond only to curve (*c*) in Fig. 6, which is not the final energy difference. A further elaborate model would demand that the BBB increment should not be constant, or that the energy difference should be given by comparing the set X—X + X—H for $H_3X{-}XH_3$ with X—H—X for $H_3X{-}H{-}XH_2$. We have an MP2 estimate for the XH bond energy, so we may evaluate the first of these two members. From the *known* final energy difference between our two isomers, we may deduce the second member, *i.e.* the *global* increment for the bond energy in X—H—X. If we set the condition that this term can in turn be decomposed into X—H + BBB′, the last *variable* increment can also be evaluated. The following terms (in kcal mol^{-1}) were all obtained from our MP2-calculated energies.

	X—H—X	variable BBB′
C	84	−21
Si	108	19
Ge	107	26
Sn	108	33
Pb	106	41

The global energy increment for the bridge is roughly constant from Si to Pb, while the BBB′ increment rises from 20 to 40 kcal mol^{-1}. We will propose elsewhere a rationale for these results, in the context of our research into simple rules for structural prediction.[22]

Saddle Points

The geometries for the saddle points are given in Table 7 (disregard for the moment column TS2). For carbon, the transition state has a staggered arrangement like **8**, with a preserved C_s symmetry. For silicon, it is also like **8**, but distorted from the C_s symmetry, the left-hand H_3Si group being rotated around Si(1)—Si(2) by only 6°. For lead, an eclipsed arrangement like **9** is found, with again preserved C_s symmetry. Note that **8** and **9** are prefigured by **7** and **6**.

Table 7 Saddle-point geometries[a]

	C	Si		Pb	Si(TS2)
X(1)—X(2)	1.942	2.418		2.933	2.541
X(1)—H_b	1.203	1.707		2.250	1.836
X(2)—H_b	1.327	1.635		1.979	1.548
X(1)—H(1)	1.082	1.468		1.477	1.468
X(1)—H(2)	1.082	1.467	1.477	1.728	1.473
X(2)—H(3)	1.097	1.481	1.481	1.767	1.507
X(1)H_bX(2)	100.2	92.7		87.6	97.0
H_bX(1)X(2)	42.3	42.5		42.4	37.2
H_bX(2)X(1)	37.6	44.8		50.0	45.8
H(1)X(1)X(2)	132.1	127.7		101.4	108.1
H(2)X(1)X(2)	96.3	101.5	99.3	108.9	110.9
H(2)X(1)H(2)	109.4	115.2		116.0	105.7
X(1)X(2)H(3)	106.3	113.1	114.7	117.3	76.0
H(3)X(2)H(3)	109.4	107.0		105.1	
H_bX(1)H_b					70.0
H_bX(2)H_b					85.8
ν_i[b]	746	547		603	413

[a] In Å and degrees. [b] Imaginary frequency (cm^{-1}).

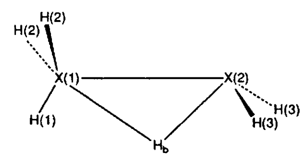

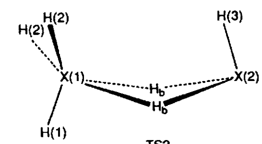

TS2

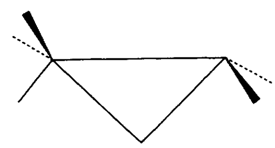

8

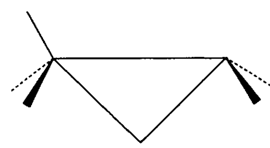

9

For silicon, our geometries are in good agreement with the transition state for the insertion of silylene into the Si—H bond of disilane, calculated by Gano *et al.* at the SCF-3-21G* level.[18] The asymmetry of the X(1)H_bX(2) three-membered ring is not the same for carbon and silicon. For carbon, the short bond in the transition state is still X(1)—H_b, while it is H_b—X(2) for silicon and lead. The relative stretches expressed in percent in the X(1)—X(2) and H_b—X(2) bonds with respect to their equilibrium values in the ethane form are 27% and 21%, respectively, for carbon, and 11% and 3%, respectively, for silicon. These results are in good agreement with the Hammond postulate since the process of $H_3X{-}XH_3$ decomposition is much more endothermic with carbon than with the other elements, implying a later transition state. Given the energy profiles of Fig. 3 and 4, we would expect for lead a transition state closer to the ethane form than that of silicon. This is not supported by the corresponding relative stretches in X(1)—X(2) and H_b—X(2) for lead, which are found to be close to those of silicon, but slightly higher.

In researching the saddle-point for Si_2H_6, a puzzling second transition state with a doubly bridged geometry like **10** has been found. This structure has C_s symmetry and corresponds to an

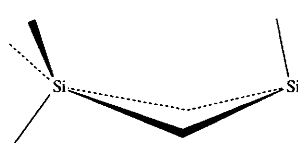

10

actual saddle point of index 1, with a single imaginary frequency. Its detailed geometry is given in Table 7 (right) referred to as TS2. This form lies 1.2 kcal mol^{-1} above the singly bridged transition state. At the MP4 level, it lies 2.4 kcal mol^{-1} below it. What does this saddle point relate to? The answer rests in the imaginary mode. Relaxing the geometry according to this a″ mode leads to the bridged structure. Relaxing it according to this mode but in the opposite direction on the path also leads to the bridged structure, but with a different bridging hydrogen. In other words, this saddle point has nothing to do with the ethane-to-bridged form pathway, and is nothing other than the transition state for hydrogen scrambling in the bridged complex, **11**.

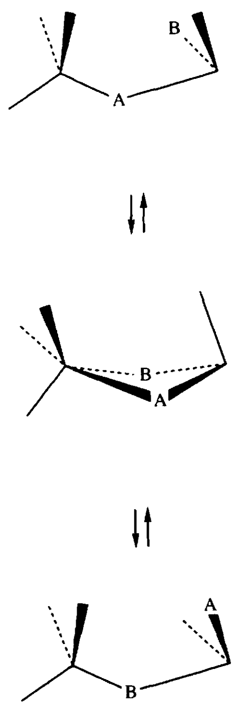

11

Our results show that this process should occur with virtually zero barrier or a very weak barrier. More accurate assessment of this transition state and of its relative energy is needed; in particular, this part of the potential surface should be explored at a correlated level of treatment. It should be noted that since the bridged complex is basically $XH_4 + XH_2$, rearrangement **11** corresponds to a hydrogen exchange between XH_4 and XH_2. The mechanism involved would therefore occur *via* the weakly bound singly bridged complex and the low doubly bridged transition state. All attempts to trap such a saddle point for C_2H_6 and Pb_2H_6 have failed so far. Because location of saddle points may be tricky, these may just have been missed, in particular for lead. Technical reasons have prevented us from performing this research for germanium and tin, but most probably this transition state should also exist on these surfaces, at least for germanium.

On the drawing of the saddle-point geometry **10**, we have not linked the two silicon atoms since no bond formation between these two atoms is concerned in the pathway. Table 7 indicates that the SiSi distance in **10** is longer than that in the other transition state, but it is much shorter than that in the bridged minimum. Linking the two atoms would have given a hexacoordinate silicon. The striking feature of this transition state is that the asymmetry in the $X-H_b$ bonds of the bridges is nearly of the same extent as that in the singly bridged complex, but is now on the opposite side, with $X(1)-H_b$ being long and $H_b-X(2)$ being short, in such a way that the system is better seen as two SiH_3 fragments in an asymetrical interaction. Clearly, the exchange of H_b requires the $X(1)-H_b$ bond to be broken.

In conclusion, we have shown in this work the existence of bound intermolecular complexes between methane-type and singlet methylene-type fragments for Group 14. As expected, such a complex is always higher than the ethane form isomer on any X_2H_6 potential surface. However, with heavier atoms, the corresponding energy difference is reduced to reach 9 kcal mol^{-1} for Pb_2H_6. This effect is paralleled with more binding with respect to the fragments $XH_4 + XH_2$ (5–10 kcal mol^{-1}), and an increasing barrier for the insertion reaction of XH_2 into XH_4. This barrier is near zero for carbon and silicon, and as large as 20 kcal mol^{-1} for lead. Once again, the potential surface appears to be less and less uniform with heavier elements.

Appendix

The calculations were performed with the HONDO8 program from the MOTECC package.[23] For all Group 14 atoms, effective core potentials were used.[24] For tin and lead atoms, these take into account the mean relativistic effects through the mass–velocity and Darwin terms.[25] The DZP valence basis sets consist of four Gaussian functions contracted to a double-zeta level and augmented by a polarization function. The exponents for the d functions are 0.80(C), 0.45(Si), 0.25(Ge), 0.20(Sn) and 0.15(Pb). The exponent for the p function on hydrogen is 0.80. The geometries are optimized at the RHF-SCF level, except for the XH_3 radicals, which are optimized at the UHF-SCF level. The final gradient components are better than 10^{-5}, except for the heavier bridged structures for which we could not go beyond 10^{-4}, even after several hundred optimization steps. The harmonic vibrational frequencies are obtained from force constants calculated by finite differences of analytical first derivatives. On each stationary point, the energy is recalculated at the MP4 level. Since Møller–Plesset calculations are not available for open shells in the MOTECC89 version of HONDO8, for the XH_3 radicals MP2 corrections to the energy were calculated by using the CIPSI program,[26] starting from OS-RHF wavefunctions. These MP2 energies were used in conjunction with the other MP2 energies, calculated with HONDO8 on the closed-shell systems, in the calculation of the dissociation energies for $H_3X-XH_3 \rightarrow 2XH_3$ and $XH_4 \rightarrow XH_3 + H$, and of the dismutation energies for $XH_4 + XH_2 \rightarrow 2XH_3$. For sake of reproducibility, we give in the following the total energies (E_h) corresponding to the zero relative energies in Table 4.

	SCF	MP4
C	−14.487 878	−14.838 330
Si	−10.996 119	−11.257 786
Ge	−10.743 397	−11.003 600
Sn	−10.047 079	−10.287 412
Pb	−10.121 879	−10.363 164

References

1 G. Treboux and G. Trinquier, *Inorg. Chem.*, 1992, **31**, 4201.
2 G. Trinquier, *J. Am. Chem. Soc.*, 1992, **114**, 6807.
3 R. Becerra, H. M. Frey, B. P. Mason, R. Walsh and M. S. Gordon, *J. Am. Chem. Soc.*, 1992, **114**, 2751.
4 J. Fernandez-Sanz and A. Marquez, *J. Phys. Chem.*, 1989, **93**, 7328.

5 H. Preut and F. Huber, *Z. Anorg. Allg. Chem.*, 1976, **419**, 92.
6 N. Kleiner and M. Drager, *J. Organomet. Chem.*, 1984, **270**, 151; 1985, **293**, 323.
7 N. Kleiner and M. Drager, *Z. Naturforsch., B:* Chem. Sci., 1985, **40**, 477.
8 R. Walsh, *Acc. Chem. Res.*, 1981, **14**, 246.
9 P. Ho, M. E. Coltrin, J. S. Binkley and C. F. Melius, *J. Phys. Chem.*, 1986, **90**, 3399.
10 B. P. Luke, J. A. Pople, M. B. Krogh-Jespersen, Y. Apeloig, J. Chandrasekhar and P. v. R. Schleyer, *J. Am. Chem. Soc.*, 1986, **108**, 206.
11 M. S. Gordon, N. T. Truong and E. K. Bonderson, *J. Am. Chem. Soc.*, 1986, **108**, 1421.
12 D. S. Horowitz and W. A. Goddard III, *J. Mol. Struct. (Theochem)*, 1988, **163**, 207.
13 A. F. Sax and J. Kalcher, *J. Phys. Chem.*, 1991, **55**, 1768.
14 K. F. Purcell and J. C. Kotz, *Inorganic Chemistry*, Saunders, Philadephia, 1977, p. 270.
15 A. F. Sax, *J. Comput. Chem.*, 1985, **6**, 469; S. Profeta, R. J. Unwalla and F. K. Cartledge, *J. Comput. Chem.*, 1989, **10**, 99.
16 P. v. R. Schleyer, M. Kaupp, F. Hampel, M. Bremer and K. Mistlow, *J. Am. Chem. Soc.*, 1992, **114**, 6791.
17 M. S. Gordon and D. R. Gano, *J. Am. Chem. Soc.*, 1984, **106**, 5421.
18 D. R. Gano, M. S. Gordon and J. A. Boatz, *J. Am. Chem. Soc.*, 1991, **113**, 6711.
19 P. M. Agrawal, D. L. Thompson and L. M. Raff, *J. Phys. Chem.*, 1990, **92**, 1069.
20 H. W. Schranz, L. M. Raff and D. L. Thompson, *J. Phys. Chem.*, 1991, **95**, 106.
21 G. Trinquier, *J. Am. Chem. Soc.*, 1990, **112**, 2130; 1991, **113**, 144; G. Trinquier and J. C. Barthelat, *J. Am. Chem. Soc.*, 1990, **112**, 9121.
22 G. Treboux and G. Trinquier, to be published.
23 M. Dupuis, MOTECC89, IBM Corporation, Center for Scientific and Engineering Computations, Kingston, NY, 12401.
24 Ph. Durand and J. C. Barthelat, *Theor. Chim. Acta*, 1975, **38**, 283.
25 J. C. Barthelat, M. Pélissier and Ph. Durand, *Phys. Rev. A*, 1981, **21**, 1773.
26 B. Huron, P. Rancurel and J. P. Malrieu, *J. Chem. Phys.*, 1973, **58**, 5475.

Paper 2/04798E; *Received 7th September*, 1992